Nano Carbons 2023; 2(1): 299.
Original Research Article

The study of ideal/defected graphene nanosheet roughness after atomic deposition process: Molecular dynamics simulation

Sedigheh Bigom Hoseini[1], Roozbeh Sabetvand[2,*]

[1] *Department of Physics, College of Sciences, Shiraz University, Shiraz, 71946-84334, Iran*

[2] *Department of Energy Engineering and Physics, Faculty of Condensed Matter Physics, Amirkabir University of Technology, Tehran, 159163-4311, Iran*

*** Corresponding author:** Roozbeh Sabetvand, r.sabetvand@gmail.com

ARTICLE INFO

Received: 8 November 2023
Accepted: 2 January 2024
Available online: 11 April 2024

doi: 10.59400/n-c.v2i1.299

ABSTRACT: In this work, a molecular dynamics (MD) approach was performed to study the surface roughness of ideal/defected graphene nanosheets after carbon atom deposition at various temperatures and pressures. In our calculations, the atomic interactions of nanostructures are based on TERSOFF and Lennard-Jones potential functions. The results show that the temperature of the simulated structure is an important parameter in the atomic deposition process, and initial temperature enlarges and intensifies the atomic deposition ratio. Numerically, by temperature increasing to 15 K, the surface roughness amplitude increases to 0.98 Å/0.83 Å after atomic deposition in ideal/defected structure. The roughness power in MD simulations converges to 0.64/0.55 in ideal/defected samples at maximum temperature. Furthermore, the pressure effects on the dynamical behavior of simulated samples were reported in our study. We conclude that, by increasing initial pressure from 0 to 2 bar, the surface roughness amplitude in ideal/defected atomic arrangements increases to 1.01 Å/0.84 Å after the deposition process, and the roughness power of simulated structures reaches a larger value. Numerically, by initial pressure setting at 2 bar, the roughness power value converged to 0.72/0.56 in ideal/defected graphene. Reported numeric results in various temperatures and pressures predicted the initial condition can be manipulated in the atomic deposition process in ideal/defected graphene nanostructures.

***KEYWORDS*:** graphene; atomic deposition; vacancy defect; molecular dynamics; temperature effect; pressure effect

1. Introduction

Graphene is the same carbon allotrope in the shape of every layer of atoms in a two-dimensional honeycomb arrangement[1,2]. It is the basic structural element of other allotropes, including graphite, charcoal, carbon nanotubes, and fullerenes. It can also be considered an indefinitely large aromatic molecule, the ultimate case of the family of flat polycyclic aromatic hydrocarbons. This atomic structure is 100 times more powerful than steel; this comparison predicted the high structural stability of graphene-based materials, which appreciably low weight. These samples have promising behavior for actual applications, such as good thermal conductivity, mechanical stability, and surface smoothness. Mechanically, this structure has an innate tensile strength of 130 GPa and a Young's modulus of 1 TPa, which can be affected by various processes such as atomic deposition[3]. However, in comparison to any

other steels, its density is significantly low, and this behavior of graphene-based structures makes them appropriate for many industrial applications. Structurally, the length of graphene's carbon–carbon bond is approximately 0.142 nm[4]. Furthermore, the sheets of graphene are piled for creating graphite with interplanar spacing of 3.35 Å. In experimental research, a big-angle-bent graphene monolayer can be attained by insignificant strain that indicates the mechanical strength of two-dimensional carbon nanostructure[5]. Atomic force microscopy (AFM) can measure the spring constant of suspended graphene sheets. For this purpose, graphene nanosheets have been suspended in SiO_2 holes in which an AFM was applied for using a stress sheet to examine the mechanical and atomic features. The range of spring constant was 1–5 N/m, and its firmness was 0.5 TPa that varies from the bulk graphite[6].

As reported before, the atomic deposition process is one of the important phenomena that can affect the mechanical and atomic properties of graphene nanosheets. Today, various methods can be implemented to study the atomic deposition process. Atomic layer deposition (ALD) is one of the common techniques for depositing processes with high precision[7]. Technically, various atomic deposition processes and their applications have developed rapidly over the last few years[8,9]. Neek-Amal et al.[10] investigated the formation of atomic nanoclusters on suspended graphene sheets in their work. They find the transition atoms aggregate and make various-sized nanoclusters distributed randomly on the graphene surface. In other work, Wang et al.[11] investigated ALD of metal oxide on graphene nanosheet. On this atomic structure, ALD coating can only actively grow on edges and defect sites, which this result shows the importance of atomic defects in the deposition process. Xuan et al.[12] presented the growth behavior of Al_2O_3 and HfO_2 films on a graphite matrix by the ALD process. They concluded the large numbers of Al_2O_3 and HfO_2 nanoribbons, with dimensions of 2000 Å and 500000 Å in width and length, respectively. Sun et al.[13] concluded the nanometric deposition of TiO_2 particles on graphene has been achieved via the ALD method.

By study of these previous researches, one can see the effect of atomic defect (vacancy) and temperature/pressure changes on the atomic deposition of graphene has not been investigated. In crystallography, a vacancy is a common type of point defect in structures where an atom is missing from one of the lattice sites[14,15]. Crystals such as graphene nanosheets possess imperfections, sometimes referred to as crystalline defects. Actually, vacancies occur naturally in all crystalline materials[16]. At any given temperature, up to the melting point of the material, there is an equilibrium concentration. In the deposition process that occurs in the graphene nanosheet, counting this atomic feature is essential. So in current work, we report these parameters (temperature/pressure variation and vacancy) effects on atomic deposition in graphene nanosheets. However, almost all prior academic papers used an experimental approach. An alternative method is the materials simulation by using an atomic model. The molecular dynamics (MD) simulations are one of the best methods for this purpose. In recent years, the MD approach has been applied to describe the atomic behavior of various materials as well as their thermodynamic and dynamical properties[17–21]. Based on previous studies that are described in this section, it is expected that the computational methods, such as MD simulation, provide an accurate tool for studying the atomic deposition in ideal/defected graphene nanosheets.

2. Computational method

MD approaches based on Newton's laws are the commonly used computational methods at the atomic scale that are currently implemented to describe the physical features of the various structures[22–26]. Computationally, this simulation approach is a precise method for tracing the time-dependent behavior of particles. In this regard, particles can be free for interactions in defined time steps, giving

the perception of the dynamical evolution of particles. In common versions of MD simulations, the particles evolution is calculated by Newton's second law, at which point the interactions between particles and their various energies are computed by potential functions. In this work, we used MD simulations with an exact atomic model to describe the roughness of ideal/defected graphene nanosheets after free carbon atom deposition processes at various initial temperatures and pressures. These calculations were done by using the LAMMPS software, version 27 February 2020, released by Sandia laboratories[27–31]. This software has various potential functions, such as Lennard-Jones (LJ), Embedded Atom Model (EAM), TERSOFF, etc. Technically, the results of the MD studies are related to potential function selection. For reaching the actual results, we should choose these computational functions appropriately. In atomic simulations of graphene, the interatomic potential for nanosheet particles was based on a TERSOFF potential[32,33]. By using this potential function, ideal and defected nanosheets have suitable structural stability before the deposition process. As a result, it is appropriate to use this potential in MD simulations of graphene samples in current research. In this computational function, the possible energy for particle arrangement is represented by a summation of distance components of interactions. The general expression of the TERSOFF potential is[22,23],

$$E = \frac{1}{2}\sum_{i}\sum_{i\neq j} V_{ij} \tag{1}$$

$$V_{ij} = f_C\left(r_{ij}\right)\left[f_R\left(r_{ij}\right) + b_{ij} f_A\left(r_{ij}\right)\right] \tag{2}$$

where f_R is a two-body term and f_A includes three-body interactions. The summations in Equation (1) are over all neighbor j and k of atom i within a cutoff distance. Furthermore, the energy between the various particles $V(r^N)$ is calculated for each pair of them. For the interatomic force between free carbon atoms and graphene nanosheets, we used LJ potential. This potential function is described as[23],

$$U(r) = 4\varepsilon[(\frac{\sigma}{r_{ij}})^{12} - (\frac{\sigma}{r_{ij}})^{6}] \tag{3}$$

where the first term of Equation (3) prevents the overlap of the particles and the second term defines the repulsive force and dipole-induced attractive interaction, respectively. Computationally, in Equation (3), r_{ij} is the distance between i and j particles. In MD simulations, ε and σ are the energy and length parameters, and these quantities depend on the type of the particles in defined structures. For C atoms, ε and σ parameters equal to 0.3050 Kcal/mol and 4.180 Å, respectively[34]. After determining the potential function for simulated structures, the MD procedure was fulfilled. To estimate the particle time evolution, Newton's second law's equation in atomic precision is implemented as the gradient of the defined potential function in Equations (4) and (5) [23].

$$F_i = \sum_{i\neq j} F_{ij} = m_i \frac{d^2 r_i}{dt^2} = m_i \frac{dv_i}{dt} \tag{4}$$

$$F_{ij} = -grad\ V_{ij} \tag{5}$$

From Equations (4) and (5), the momentum P_i can be calculated as[23],

$$P_i = m_i v_i \tag{6}$$

So, total energy (E) of atomic arrangement can be expressed in the form of Hamilton as Equation (7)[23],

$$\mathrm{H}(r,P)=\frac{1}{2m}\sum_{i}P_i^2+V(r_1+r_2+\cdots+r_n)=E \tag{7}$$

Furthermore, Gaussian distribution is used for calculating the particles temperature as Equation (8)[23],

$$\frac{3}{2}k_BT=\frac{1}{N_{atom}}\sum_{i=1}^{N}\frac{1}{2}mv_i^2 \tag{8}$$

So, the temperature fluctuates is estimated by Equation (9)[23],

$$T(t)=\sum_{i}^{N}\frac{m_iv_i^2(t)}{k_BN_{sf}} \tag{9}$$

where, N_{sf} is the freedom degree of atomic structure. Association of motion equations is done by velocity Verlet formalism for integrating the Newton's law that is shown below[35,36],

$$r(t+\delta t)=r(t)+v(t)\delta t+\frac{1}{2}a(t)\delta t^2 \tag{10}$$

$$v(t+\delta t)=v(t)+\frac{1}{2}[a(t)+a(t+\delta t)]\delta t \tag{11}$$

In Equations (10) and (11), and refer to the coordinates and velocities of particles, respectively. Also, and refer to the initial value of these physical parameters. Technically, various thermostats/barostats are used to set initial conditions in MD simulations. The Nose-Hoover thermostat/barostat is one of the deterministic algorithms for temperature/pressure control in common MD simulations[37,38]. So, the Nose-Hoover formalism has been applied as a precise process for constant temperature/pressure simulations. Currently, this simulation mechanism is implemented to access the equilibrium phase for 5 ns, but MD simulations were carried out until 5 ns later for the free carbon atom deposition process. We can say the atomic simulations in our computational work consist of two steps:

Step A) Pressure effect on surface roughness of ideal/defected graphene nanosheet after free carbon atoms deposition

Firstly, ideal/defected graphene nanosheets were modeled inside the box with lx = ly = lz = 120 Å lengths. In this computational box, periodic boundary conditions were used in the x and y directions, while the z direction was fixed. Then, Nose-Hoover formalism was used for the atomic samples to equilibrate particles at various pressures (P = 0, 1 bar, and 2 bar). Also, the atomic defect ratio in non-ideal nanosheets is set to 2.5%, 5%, and 10%. By these defect settings, the number of missed carbon atoms inside nanosheets is 245, 490, and 980, respectively. By defining these numerical values, the effect of the vacancy defect in the atomic deposition on graphene-based samples is determined. Simultaneously, the designed atomic samples have good atomic stability in defined initial conditions. Afterward, the system reaches an equilibrium phase, free carbon atom deposition is done, and the atomic behavior of the graphene nanosheet is reported by surface roughness amplitude and roughness power parameters calculation. For the described process, 450, 650, and 850 numbers of free carbon atoms were deposited on ideal/defected nanosheets. By using these numbers of free atoms, the physical stability in samples isn't destructed, and the deposition process is detected obviously.

Step B) Temperature effect on surface roughness of ideal/defected graphene nanosheet after free carbon atoms deposition

In the second step, the thermodynamic equilibration and atomic stability of graphene nanosheets were simulated at various initial temperatures (T = 5 K, 10 K, and 15 K). After equilibration process detection, free carbon atom deposition on ideal/defected graphene nanosheets was done, and atomic behavior of simulated structures was reported as described in step A.

3. Results and discussion

3.1. Pressure effect on surface roughness of ideal/defected graphene nanosheet after free carbon atoms deposition

In the first step, the graphene nanosheets with ideal and defected atomic arrangements were simulated. These nanostructures are depicted in **Figure 1**. For atomic analysis of graphene atom behavior after free carbon atom deposition in a simulation box, the physical parameters such as total energy, temperature, amplitude of surface roughness, and roughness power were reported, and these quantities were compared with each other at various initial pressures. From MD simulation results, we can say the graphene nanosheet temperature converged to 5 K after 5 ns in ideal and defected arrangements. Furthermore, as shown in **Figure 2**, the total energy of ideal/defected nanosheet converged to a finite value after this simulation time. From numerical averaging of this physical quantity, we concluded the energy of ideal/defected structure reached -7.32 eV/-6.76 eV for each atom. This total energy variation of nanostructures shows that the carbon atoms inside the graphene nanosheet have the structural stability that was reported in previous publications and shows our MD method's validity[23]. Physically, this calculation shows the ideal/defected graphene nanosheet has atomic stability in T = 5 K and P = 0, 1 bar, and 2 bar. Furthermore, our results from this section show the carbon atom's position and TERSOFF potential are well matched with each other. Technically, these computational results represent the minimum number of MD simulation time steps needed to equilibrate graphene nanosheets. After the atomic equilibrium process, in all samples, graphene was deposited by free carbon atoms (with 10 eV energy). The number of free particles is one of the important parameters in the deposition process. This parameter effect was studied with roughness amplitude (W) calculation. The roughness amplitude estimated by Equation (12),

$$W = \frac{1}{N}\sqrt{\sum_{i\neq j=1}^{N}(h(i,j)-< h(i,j) >)^2} \tag{12}$$

where,

$$< h(i,j) >= \frac{1}{N^2}\sum_{i\neq j=1}^{N} h(i,j) \tag{13}$$

In Equation (13), N is the number of atoms, and h represents the height of the atomic roughness. By using 450, 650, and 850 numbers of free carbon atoms in the deposition process, the amplitude of surface roughness reaches 0.55 Å, 0.58 Å, and 0.59 Å, respectively (for ideal graphene). Furthermore, roughness power reached 0.53, 0.58, and 0.61 for the reported number of free carbon atoms. So, free atoms increasing in the ideal graphene deposition process cause the increase in the surface roughness of the nanosheet. This atomic behavior arises from the interaction between the simulated nanosheet and free atoms. Physically, as the number of free atoms in deposition process increases, the amount of attraction force which applied to the nanosheet get bigger and cause the roughness amplitude and roughness power of graphene nanosheet increasing.

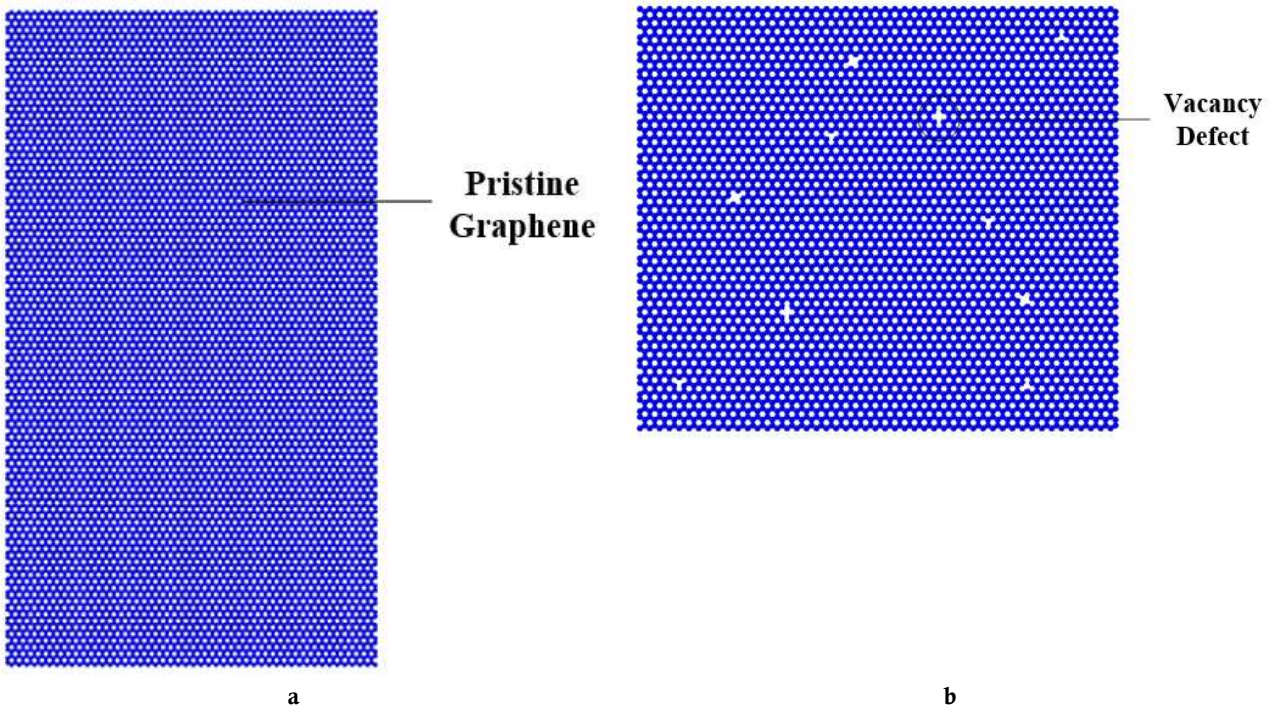

Figure 1. Atomic representation of **a)** ideal and **b)** defected graphene nanosheets in current computational study.

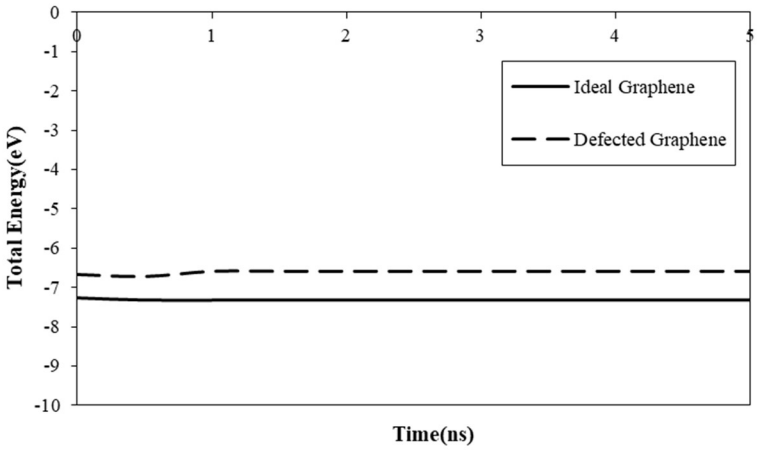

Figure 2. Total energy/atom changes of ideal and defected (with 5% atomic ratio) graphene nanosheet at P = 0 and T = 5 K, as a function of simulation time.

Next, we deposited free carbon atoms on an ideal graphene nanosheet at various pressures (equal to 0, 1 bar, and 2 bar). By these initial pressure settings, free atoms deposited on the graphene nanosheet surface successfully (see **Figure 3**). As mentioned before, the surface roughness amplitude and roughness power of free carbon atoms show the deposition process properties in our MD simulations. The variation of these physical parameters as a function of MD simulation time is depicted in **Figures 4–6**. From these figures, we concluded the atomic deposition process occurs after 5 ns for various pressures. Numerically, by increasing MD simulation pressure, the surface roughness amplitude of the ideal nanosheet increased, and the maximum value of this parameter reached 1.01 Å at 2 bar pressure, as reported in **Table 1**. Furthermore, roughness power of the simulated structure at P = 2 bar and T = 5 K reaches 0.72 (see **Figure 6** and **Table 2**). This atomic behavior arises from atomic interaction increasing by pressure changes from 0 to 2 bar. Physically, by pressure increasing, the

interatomic distance between free atoms and ideal graphene decreases in the final step of the simulation. So, by interatomic distance decreasing, the potential energy converged to bigger values, and atomic attraction reached its maximum value.

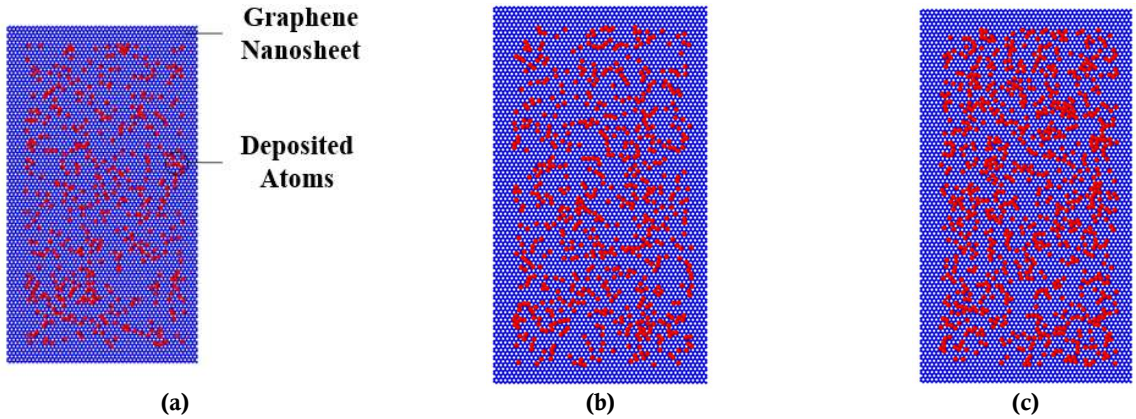

Figure 3. Atomic deposition process in ideal graphene nanosheet as a function of free carbon atoms number with: **a)** 450, **b)** 650, and **c)** 850 atoms.

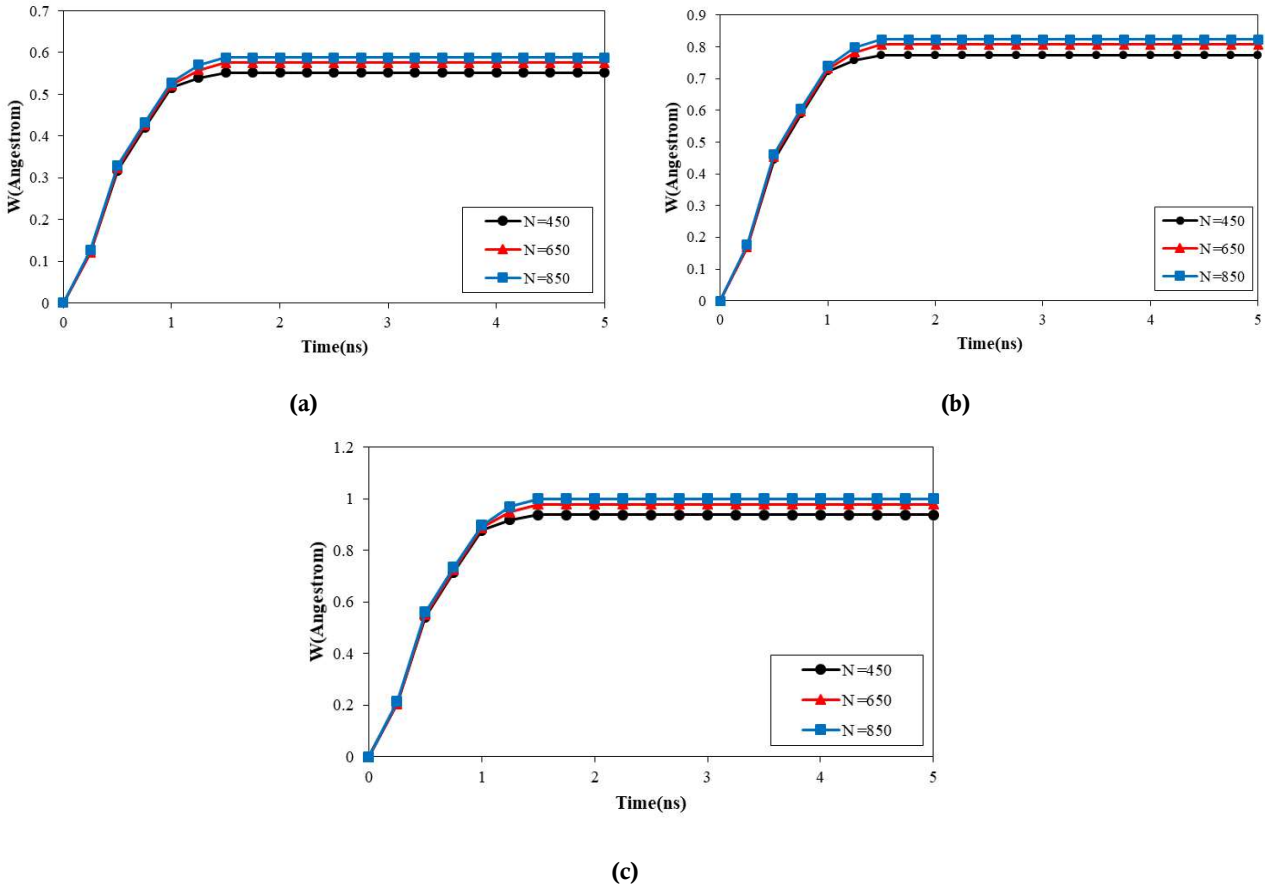

Figure 4. Surface roughness amplitude of ideal graphene nanosheet after atomic deposition process at: **a)** P = 0, **b)** P = 1 bar, and **c)** P = 2 bar as a function of free carbon atoms numbers and simulation time.

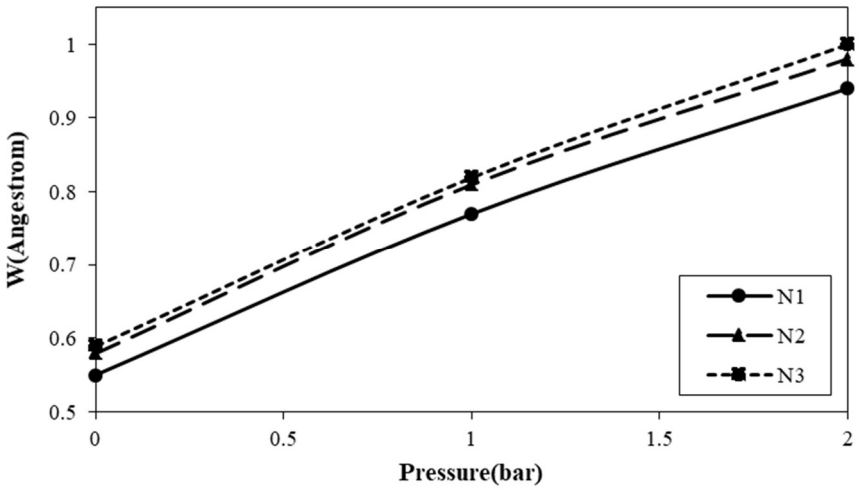

Figure 5. Surface roughness amplitude of ideal graphene nanosheet after atomic deposition process as a function of initial pressure and free carbon atoms numbers (N1 = 450, N2 = 650, and N3 = 850 atoms).

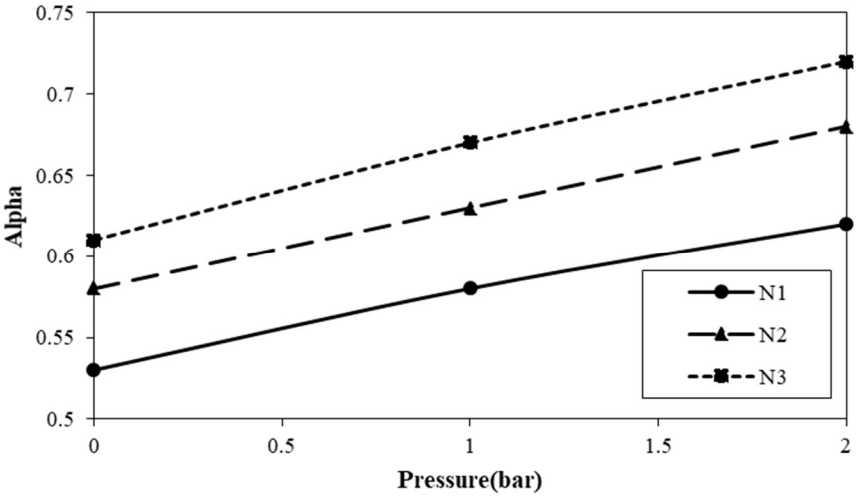

Figure 6. Roughness power of ideal graphene nanosheet after atomic deposition process as a function of free carbon atoms numbers (N1 = 450, N2 = 650, and N3 = 850 atoms) and initial pressure.

Table 1. Maximum value of surface roughness amplitude of ideal graphene nanosheet after deposition process as a function of initial pressure and number of free carbon atoms.

Pressure (bar)	Maximum value for 450 atoms (Å)	Maximum value for 650 atoms (Å)	Maximum value for 850 atoms (Å)
0	0.55	0.58	0.59
1	0.77	0.81	0.82
2	0.94	0.98	1.01

Table 2. Roughness power of ideal graphene nanosheet after deposition process as a function of initial pressure and number of free carbon atoms.

Pressure (bar)	Maximum value for 450 atoms (Å)	Maximum value for 650 atoms (Å)	Maximum value for 850 atoms (Å)
0	0.53	0.58	0.61
1	0.58	0.63	0.67
2	0.62	0.68	0.72

Next, vacancy defects with 2.5%, 5%, and 10% atomic ratios were implemented in pristine nanosheets. As depicted in **Figures 7** and **8**, by this parameter increasing, the surface roughness amplitude and roughness power of the simulated nanosheet after atomic deposition decrease. Physically, these calculated parameters show the effective interaction between free carbon atoms and defected graphene nanosheets decreases rather than ideal ones. By an atom missing in pristine graphene, the interaction space for the deposition process enlarges, and atomic disorder in the MD simulation box decreases. Numerically, by vacancy ratio changes, the minimum value of surface roughness amplitude in simulated structures changes reached 0.47 Å. Furthermore, the final value of roughness power decreased to 0.47 by vacancy defect ratio enlarging.

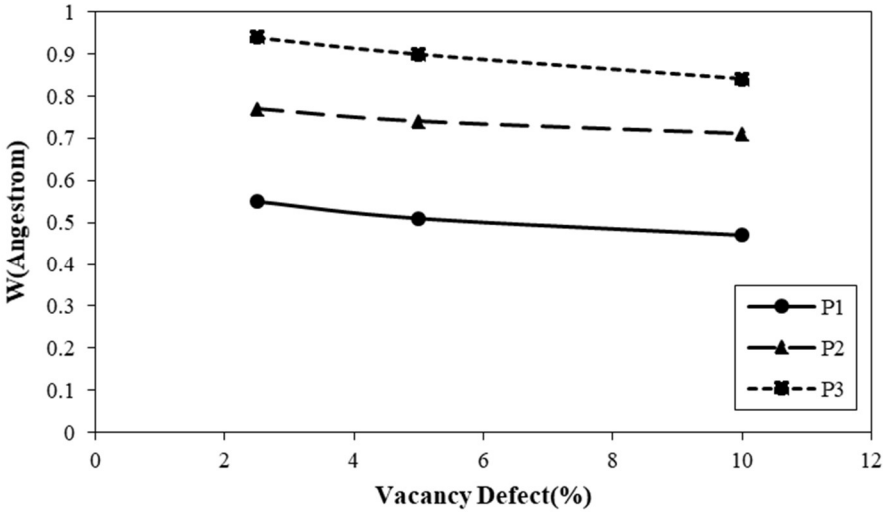

Figure 7. Surface roughness amplitude of defected graphene nanosheet after atomic deposition process as a function of defect ratio and initial pressure (P1 = 0, P2 = 1 bar, and P3 = 2 bar).

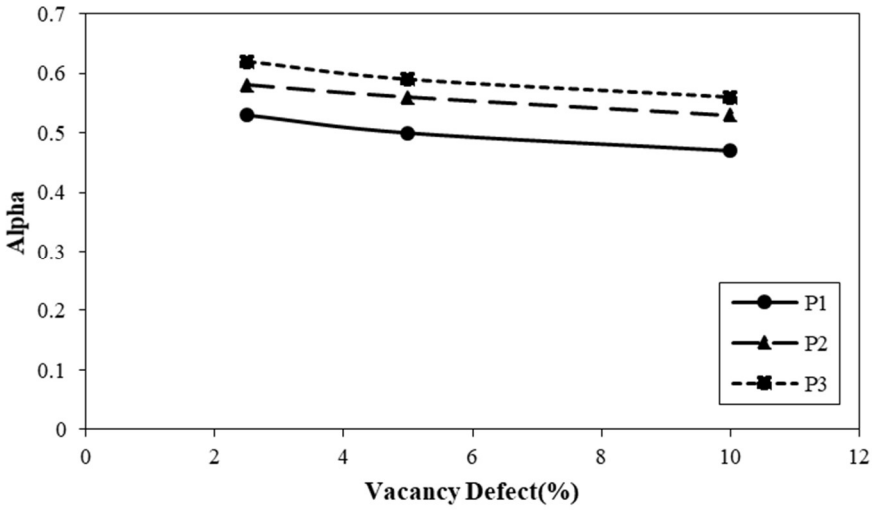

Figure 8. Roughness power of defected graphene nanosheet after atomic deposition process as a function of defect ratio and initial pressure (P1=0, P2=1 bar, and P3=2 bar).

3.2. Temperature effect on surface roughness of ideal/defected graphene nanosheet after free carbon atoms deposition

In the second step of our computational study, the effect of initial temperature on the atomic deposition process is reported. For this purpose, ideal/defected nanosheet temperature equilibrated at 5

K, 10 K, and 15 K. **Figures 9** and **10** depicted the temperature and total energy changes of atomic structures as a function of MD simulation time. From calculated results, we can say the temperature of various structures equilibrated at initial temperature after 5 ns. So, 5,000,000 time steps are sufficient for equilibration process detection in our MD simulations. Furthermore, **Figure 9** shows that the total energy of atomic structures varies with temperature changes, and this physical parameter has a direct relation with the temperature of atoms. Physically, the atomic fluctuations increased by temperature enlarging. This atomic behavior arises from interatomic distance enlarging by temperature increasing, and so the potential/total energy of simulated structures decreases. From this figure, we concluded the temperature variation changes the total energy of ideal/defected nanosheets, and so this phenomenon causes notable variation in the atomic behavior of modeled nanosheets. Numerically, the total energy of ideal/defected nanosheets decreased to −6.32 eV/−6.49 eV by temperature increasing to 15 K.

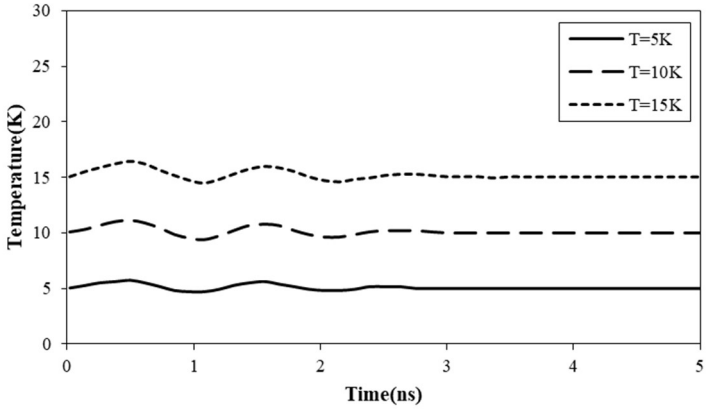

Figure 9. Temperature changes of ideal graphene nanosheet (at P = 0) as a function of initial temperature and simulation time.

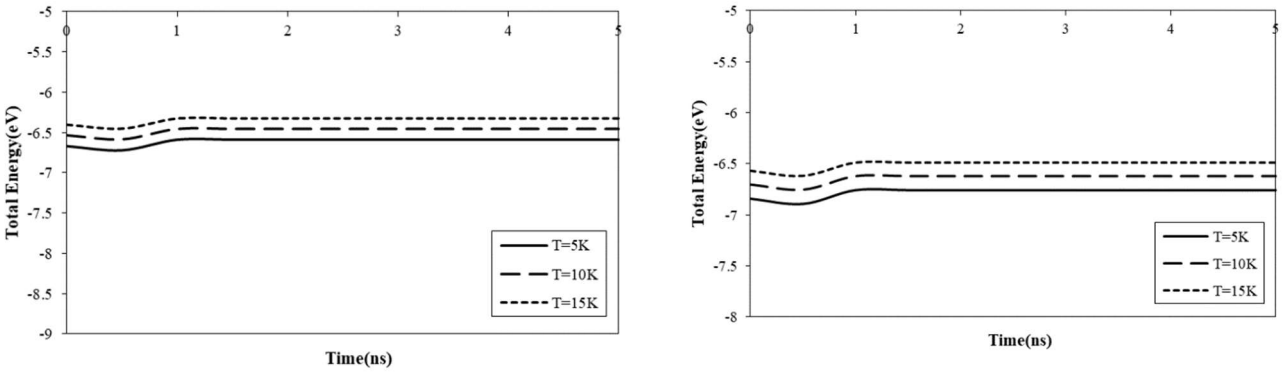

(a) **(b)**

Figure 10. Total energy/atom changes of **a)** ideal and **b)** defected (with 2.5% atomic ratio) graphene nanosheets at P = 0, as a function of initial temperature and simulation time.

After equilibration phase detection, free carbon atoms deposited on ideal graphene nanosheets at P = 0 with 10 eV energy. Our MD results indicated the graphene nanosheet stability decreased with increasing temperature. Numerically, the maximum value of surface roughness amplitude converged to 0.98 Å at T = 15 K as reported in **Table 3**. These phenomena occur because atomic fluctuations of C atoms increase in graphene nanosheets at higher temperatures. So, we concluded the atomic interaction between ideal nanosheets and free carbon atoms decreases in this simulation procedure. Finally, by

interatomic force decreasing, the atomic displacement value increased. By temperature enlarging to T = 15 K, roughness power of ideal graphene nanosheet increased to 0.64 as listed in **Table 4**. Roughness amplitude and roughness power variations as a function of MD simulation temperature are reported in **Figures 11** to **13**. By study of these calculated results, we concluded the atomic stability of simulated structures decreased by increasing initial temperature, and roughness of ideal nanosheet reached a higher value after the deposition process.

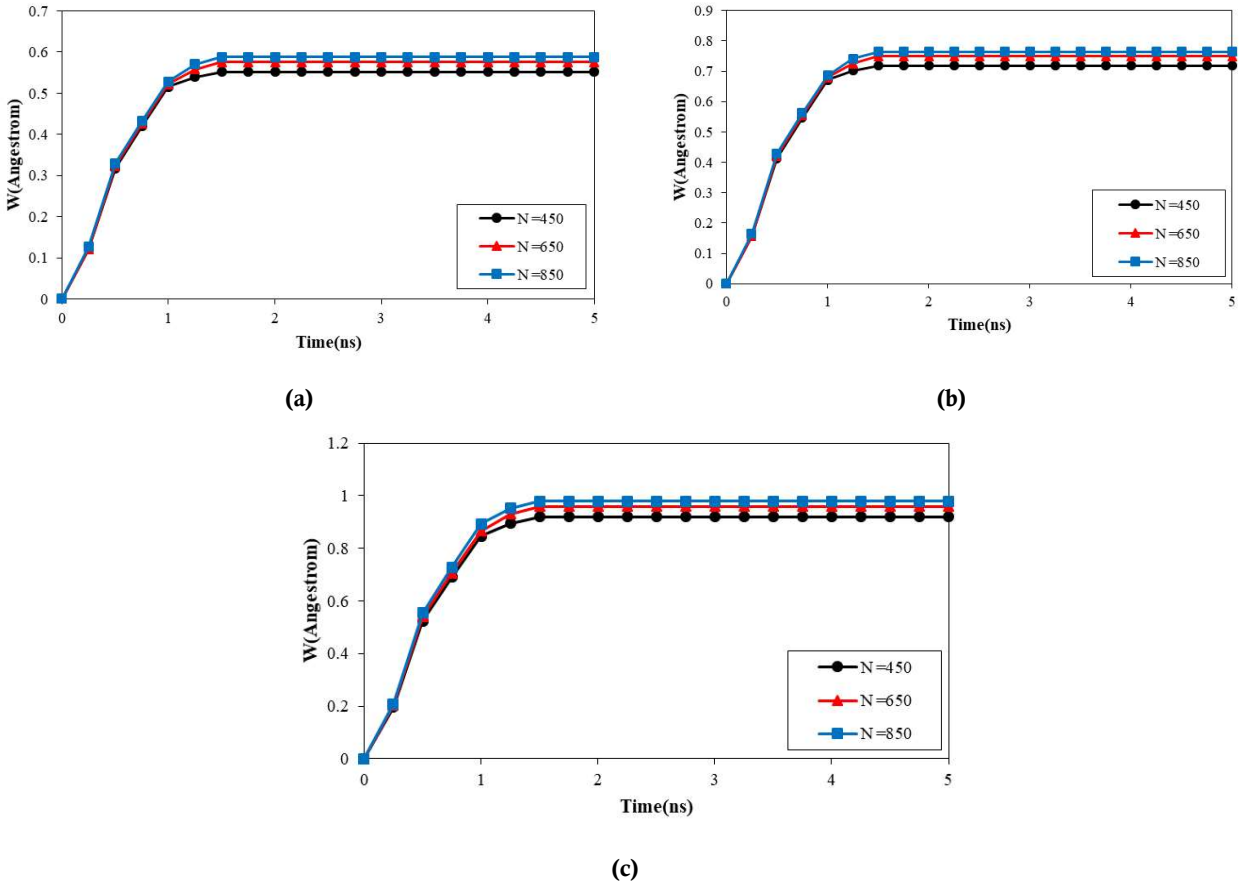

Figure 11. Surface roughness amplitude of graphene nanosheet after atomic deposition process at: **a)** T = 5 K, **b)** T = 10 K, and **c)** T = 15 K as a function of free carbon atoms number and simulation time.

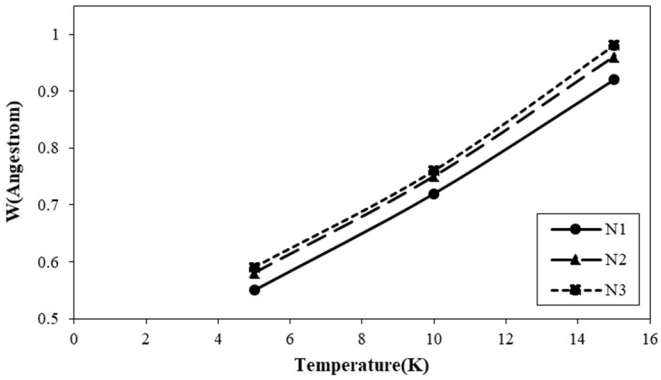

Figure 12. Surface roughness amplitude of graphene nanosheet after atomic deposition process changes as a function of free carbon atoms numbers (N1 = 450, N2 = 650, and N3 = 850 atoms) and initial temperature.

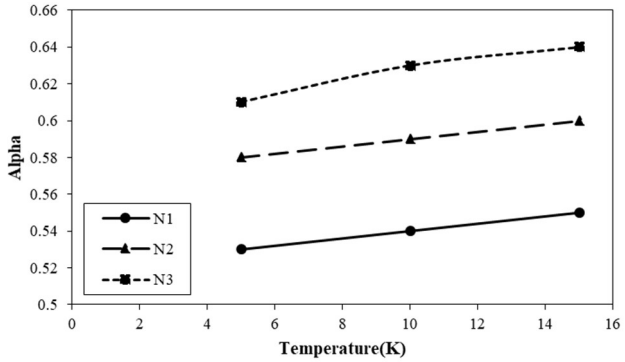

Figure 13. Roughness power of graphene nanosheet after atomic deposition process changes as a function of free carbon atoms numbers (N1 = 450, N2 = 650, and N3 = 850 atoms) and initial temperature.

Table 3. Maximum value of surface roughness amplitude of graphene nanosheet changes after deposition process as a function of initial temperature.

Temperature (K)	Maximum value for 450 atoms (Å)	Maximum value for 650 atoms (Å)	Maximum value for 850 atoms (Å)
5	0.55	0.58	0.59
10	0.72	0.75	0.76
15	0.92	0.96	0.98

Table 4. Roughness power of graphene nanosheet after deposition process changes as a function of initial temperature.

Temperature (K)	Maximum value for 450 atoms (Å)	Maximum value for 650 atoms (Å)	Maximum value for 850 atoms (Å)
5	0.53	0.58	0.61
10	0.54	0.59	0.63
15	0.55	0.6	0.64

Vacancy defects were implemented in our MD simulations in this step of our computational work. As reported before, by carbon atoms missing in pristine graphene nanosheet, the atomic order of free particles on nanosheet increased. This atomic phenomenon arises from proper placement of free atoms in defected graphene. Structurally, vacancy defects created vacant sites inside nanosheets, and the repulsive force between free carbon atoms and nanosheet particles decreased. So, the adsorption of free atoms on defected nanosheets intensified rather than ideal graphene. Numerically, by vacancy defect ratio, the maximum value of surface roughness amplitude decreased to 0.48 Å as listed in **Figure 14**. Furthermore, roughness power decreased to 0.49 (see **Figure 15**), which this variation arises from atomic order enlarging and decreases of free atom accumulation after the deposition process.

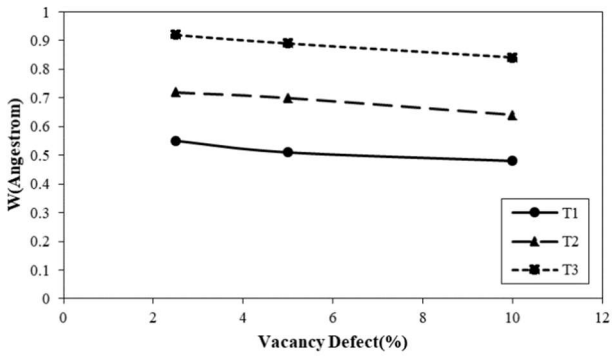

Figure 14. Surface roughness amplitude of defected graphene nanosheet after atomic deposition process changes as a function of vacancy ratio and initial temperature (T1 = 5 K, T2 = 10 K, and T3 = 15 K).

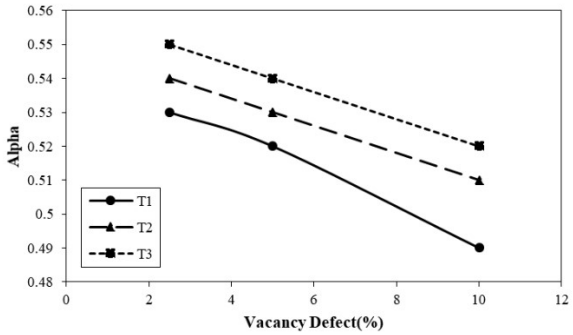

Figure 15. Roughness power of defected graphene nanosheet after atomic deposition process changes as a function of vacancy ratio and initial temperature (T1 = 5 K, T2 = 10 K, and T3 = 15 K).

In the final step of our MD study, the interaction energy between deposed atoms and pristine graphene nanosheet was reported. This physical parameter indicated the atomic evolution of simulated structures. We reported the simple and angular components of interaction energy in **Tables 5** and **6**. MD results show that by inserting a vacancy defect into a pristine nanosheet, the interaction energy between free carbon atoms and the graphene nanosheet increased. This behavior arises from atomic distance decreasing between simulated components, which, by this atomic evolution, increased the stability of structures. As reported in **Tables 5** and **6**, vacancy defect caused interaction energy enlarging to −0.182 eV for atomic systems at T = 5 K and P = 0. Furthermore, temperature/pressure increasing can affect the interaction energy in the simulated structure and decrease/increase the interaction energies. Numerically, by temperature/pressure increasing, the interaction energy reached −0.144 eV/ −0.184 eV. These calculated results introduced the importance of initial temperature and pressure changes in free carbon atoms and nanosheet interactions, which can affect the physical stability of designed atomic systems in current research.

Table 5. The interaction energy/atom between ideal graphene nanosheet and free carbon atoms as a function of temperature and pressure after t = 5 ns.

	Interaction energy/atom (eV)	
Temperature (K)/pressure (bar)	**Simple term**	**Angle term**
T = 5/P = 0	−0.139	−0.024
T = 10/P = 0	−0.131	−0.022
T = 15/P = 0	−0.124	−0.02
T = 5/P = 1	−0.149	−0.028
T = 5/P = 2	−0.153	−0.031

Table 6. The interaction energy/atom between defected graphene nanosheet (with 2.5% vacancy) and free carbon atoms as a function of temperature and pressure after t = 5 ns.

	Interaction energy/atom(eV)	
Temperature (K)/pressure (bar)	**Simple term**	**Angle term**
T = 5/P = 0	−0.157	−0.025
T = 10/P = 0	−0.152	−0.022
T = 15/P = 0	−0.147	−0.021
T = 5/P = 1	−0.16	−0.029
T = 5/P = 2	−0.168	−0.032

4. Conclusion

Molecular dynamics (MD) approaches have been used to study the initial pressure and temperature effects on ideal/defected graphene nanosheet roughness after the atomic deposition process. Technically, temperature, total energy, roughness amplitude, and roughness power parameters are reported for deposition process analysis. The results from our MD simulations indicated the atomic structures have higher stability at high/low values of initial pressure/temperature. Furthermore, we concluded the atomic order of pristine structures after the deposition process affected by pressure and temperature changes. The number of free carbon atoms and vacancy defects in the deposition process are other important parameters in our computational study. Numerically, we can say that:

- By the number of free atoms (carbon atoms) increasing in the deposition process from 450 to 850 atoms, the amplitude of the graphene nanosheet changes from 0.94 Å to 1.01 Å.
- By the number of free carbon atoms increasing in the deposition process, the maximum value of roughness power converged to a value of 0.72.
- Pressure is an important parameter in the atomic deposition process. Our calculation shows the amplitude of surface roughness in the graphene nanosheet converged to 1 Å by pressure increasing to 2 bar.
- Maximum value of roughness power (0.72) calculated for atomic structures with 2 bar pressure.
- Surface roughness amplitude is proportional to initial temperature, and this physical parameter reached 0.98 Å at T = 15 K.
- The maximum value of roughness power is 0.64, which is calculated for atomic structures at T = 15 K.
- By vacancy defect increasing to 10%, the surface roughness amplitude and value of roughness power decreased to 0.47 Å and 0.47, respectively. This minimum value is calculated for maximum initial pressure (P = 2 bar) and minimum temperature (T = 5 K). So, pressure decreasing caused roughness amplitude and value of roughness power increasing.
- By initial temperature increasing in defected graphene nanosheet with a 10% atomic ratio, the surface roughness amplitude and value of roughness power increased.

These numerical results from our MD simulations can be used in actual applications for manipulation of the atomic deposition process effects on various nanosheets.

Availability of data and material

Data available on request from the authors.

Code availability

LAMMPS main input available on request from the authors.

Author contributions

Designed the analysis, performed the analysis, wrote the paper, SBH; designed the analysis, proofread, RS. All authors have read and agreed to the published version of the manuscript.

Conflict of interest

The authors declare that they have no conflicts of interest.

Greek symbols

ε Energy parameter of Lennard-Jones function (eV/ Å)

σ Length parameter of Lennard-Jones function (Å)

δt Time step of simulation (ps)

α Atomic roughness power

Nomenclature

F_{ij} Force between i and j particles (eV/Å)

V_{ij} Potential function (eV)

m Mass of particles (u)

r_c Cut-off radius (Å)

r_{ij} Distance between i and j particles (Å)

k_B Boltzmann constant (eV/K)

T Temperature (K)

v Particles velocity (Å/ps)

N_{atom} Number of particles

H Hamiltonian of particles

W Amplitude of atomic roughness

References

1. Geim AK. Graphene: Status and Prospects. Science. 2009, 324(5934): 1530-1534. doi: 10.1126/science.1158877
2. Lee C, Wei X, Kysar JW, et al. Measurement of the Elastic Properties and Intrinsic Strength of Monolayer Graphene. Science. 2008, 321(5887): 385-388. doi: 10.1126/science.1157996
3. Ansari R, Mirnezhad M, Rouhi H. Mechanical properties of fully hydrogenated graphene sheets. Solid State Communications. 2015, 201: 1-4. doi: 10.1016/j.ssc.2014.10.002
4. Georgantzinos SK, Giannopoulos GI, Anifantis NK. Numerical investigation of elastic mechanical properties of graphene structures. Materials & Design. 2010, 31(10): 4646-4654. doi: 10.1016/j.matdes.2010.05.036
5. Gao Y, Hao P. Mechanical properties of monolayer graphene under tensile and compressive loading. Physica E: Low-dimensional Systems and Nanostructures. 2009, 41(8): 1561-1566. doi: 10.1016/j.physe.2009.04.033
6. Bu H, Chen Y, Zou M, et al. Atomistic simulations of mechanical properties of graphene nanoribbons. Physics Letters A. 2009, 373(37): 3359-3362. doi: 10.1016/j.physleta.2009.07.048
7. Memarian F, Fereidoon A, Darvish Ganji M. Graphene Young's modulus: Molecular mechanics and DFT treatments. Superlattices and Microstructures. 2015, 85: 348-356. doi: 10.1016/j.spmi.2015.06.001
8. Vervuurt RHJ, Kessels WMM (Erwin), Bol AA. Atomic Layer Deposition for Graphene Device Integration. Advanced Materials Interfaces. 2017, 4(18). doi: 10.1002/admi.201700232
9. Zhang Y, Ren W, Jiang Z, et al. Low-temperature remote plasma-enhanced atomic layer deposition of graphene and characterization of its atomic-level structure. J Mater Chem C. 2014, 2(36): 7570-7574. doi: 10.1039/c4tc00849a
10. Neek-Amal M, Asgari R, Rahimi Tabar MR. The formation of atomic nanoclusters on graphene sheets. Nanotechnology. 2009, 20(13): 135602. doi: 10.1088/0957-4484/20/13/135602
11. Wang X, Tabakman SM, Dai H. Atomic Layer Deposition of Metal Oxides on Pristine and Functionalized Graphene. Journal of the American Chemical Society. 2008, 130(26): 8152-8153. doi: 10.1021/ja8023059
12. Xuan Y, Wu YQ, Shen T, et al. Atomic-layer-deposited nanostructures for graphene-based nanoelectronics. Applied Physics Letters. 2008, 92(1). doi: 10.1063/1.2828338
13. Sun X, Xie M, Wang G, et al. Atomic Layer Deposition of TiO2on Graphene for Supercapacitors. Journal of The Electrochemical Society. 2012, 159(4): A364-A369. doi: 10.1149/2.025204jes
14. Hong J, Hu Z, Probert M, et al. Exploring atomic defects in molybdenum disulphide monolayers. Nature Communications. 2015, 6(1). doi: 10.1038/ncomms7293

15. Ehrhart P. Properties and interactions of atomic defects in metals and alloys. In: Landolt-Börnstein, New Series III, Volume 25. Springer, Berlin. 1991.
16. Siegel RW. Vacancy concentrations in metals. Journal of Nuclear Materials. 1978, 69-70: 117-146. doi: 10.1016/0022-3115(78)90240-4
17. Jolfaei NA, Jolfaei NA, Hekmatifar M, et al. Investigation of thermal properties of DNA structure with precise atomic arrangement via equilibrium and non-equilibrium molecular dynamics approaches. Computer Methods and Programs in Biomedicine. 2020, 185: 105169. doi: 10.1016/j.cmpb.2019.105169
18. Pishkenari HN, Afsharmanesh B, Tajaddodianfar F. Continuum models calibrated with atomistic simulations for the transverse vibrations of silicon nanowires. International Journal of Engineering Science. 2016, 100: 8-24. doi: 10.1016/j.ijengsci.2015.11.005
19. Toghraie D, Hekmatifar M, Salehipour Y, et al. Molecular dynamics simulation of Couette and Poiseuille Water-Copper nanofluid flows in rough and smooth nanochannels with different roughness configurations. Chemical Physics. 2019, 527: 110505. doi: 10.1016/j.chemphys.2019.110505
20. Albooyeh AR, Dadrasi A, Mashhadzadeh AH. Effect of point defects and low-density carbon-doped on mechanical properties of BNNTs: A molecular dynamics study. Materials Chemistry and Physics. 2020, 239: 122107. doi: 10.1016/j.matchemphys.2019.122107
21. Zhou YP, Jiang JW. Molecular dynamics simulations for mechanical properties of borophene: parameterization of valence force field model and Stillinger-Weber potential. Scientific Reports. 2017, 7(1). doi: 10.1038/srep45516
22. Board JA, Causey JW, Leathrum JF, et al. Accelerated molecular dynamics simulation with the parallel fast multipole algorithm. Chemical Physics Letters. 1992, 198(1-2): 89-94. doi: 10.1016/0009-2614(92)90053-p
23. Rapaport DC. The Art of Molecular Dynamics Simulation. Published online April 1, 2004. doi: 10.1017/cbo9780511816581
24. Alder BJ, Wainwright TE. Studies in Molecular Dynamics. I. General Method. The Journal of Chemical Physics. 1959, 31(2): 459-466. doi: 10.1063/1.1730376
25. Rahman A. Correlations in the Motion of Atoms in Liquid Argon. Physical Review. 1964, 136(2A): A405-A411. doi: 10.1103/physrev.136.a405
26. Gibson JB, Goland AN, Milgram M, et al. Dynamics of Radiation Damage. Physical Review. 1960, 120(4): 1229-1253. doi: 10.1103/physrev.120.1229
27. Plimpton SJ, Thompson AP. Computational aspects of many-body potentials. MRS Bulletin. 2012, 37(5): 513-521. doi: 10.1557/mrs.2012.96
28. Plimpton SJ, Pollock R, Stevens M. In: Proc of the Eighth SIAM Conference on Parallel Processing for Scientific Computing, Minneapolis, MN 223-245. 1997.
29. Brown WM, Wang P, Plimpton SJ, et al. Implementing molecular dynamics on hybrid high performance computers—Short range forces. Computer Physics Communications. 2011, 182(4): 898-911. doi: 10.1016/j.cpc.2010.12.021
30. Parks ML, Lehoucq RB, Plimpton SJ, et al. Implementing peridynamics within a molecular dynamics code. Computer Physics Communications. 2008, 179(11): 777-783. doi: 10.1016/j.cpc.2008.06.011
31. Mukherjee RM, Crozier PS, Plimpton SJ, et al. Substructured molecular dynamics using multibody dynamics algorithms. International Journal of Non-Linear Mechanics. 2008, 43(10): 1040-1055. doi: 10.1016/j.ijnonlinmec.2008.04.003
32. Tersoff J. Modeling solid-state chemistry: Interatomic potentials for multicomponent systems. Physical Review B. 1989, 39(8): 5566-5568. doi: 10.1103/physrevb.39.5566
33. Tersoff J. New empirical approach for the structure and energy of covalent systems. Physical Review B. 1988, 37(12): 6991-7000. doi: 10.1103/physrevb.37.6991
34. Rappe AK, Casewit CJ, Colwell KS, et al. UFF, a full periodic table force field for molecular mechanics and molecular dynamics simulations. Journal of the American Chemical Society. 1992, 114(25): 10024-10035. doi: 10.1021/ja00051a040
35. Verlet L. Computer "Experiments" on Classical Fluids. I. Thermodynamical Properties of Lennard-Jones Molecules. Physical Review. 1967, 159(1): 98-103. doi: 10.1103/physrev.159.98
36. Press WH, Teukolsky SA, Vetterling WT, Flannery BP. Second-Order Conservative Equations. Numerical Recipes: The Art of Scientific Computing, 3rd ed. Cambridge University Press. 2007.
37. Nosé S. A unified formulation of the constant temperature molecular dynamics methods. The Journal of Chemical Physics. 1984, 81(1): 511-519. doi: 10.1063/1.447334
38. Hoover WG. Canonical dynamics: Equilibrium phase-space distributions. Physical Review A. 1985, 31(3): 1695-1697. doi: 10.1103/physreva.31.1695